ANNUAL REVIEWS

Annual Review of Biochemistry

Soluble Methane Monooxygenase

Rahul Banerjee, Jason C. Jones, and John D. Lipscomb

Department of Biochemistry, Molecular Biology, and Biophysics, University of Minnesota, Minneapolis, Minnesota 55455, USA; email: baner025@umn.edu, jone2616@umn.edu, lipsc001@umn.edu

Annu. Rev. Biochem. 2019. 88:409–31

First published as a Review in Advance on January 11, 2019

The *Annual Review of Biochemistry* is online at biochem.annualreviews.org

https://doi.org/10.1146/annurev-biochem-013118-111529

Keywords

methane, monooxygenase, oxygen activation, kinetics, crystallography, spectroscopy

Abstract

Aerobic life is possible because the molecular structure of oxygen (O_2) makes direct reaction with most organic materials at ambient temperatures an exceptionally slow process. Of course, these reactions are inherently very favorable, and they occur rapidly with the release of a great deal of energy at high temperature. Nature has been able to tap this sequestered reservoir of energy with great spatial and temporal selectivity at ambient temperatures through the evolution of oxidase and oxygenase enzymes. One mechanism used by these enzymes for O_2 activation has been studied in detail for the soluble form of the enzyme methane monooxygenase. These studies have revealed the step-by-step process of O_2 activation and insertion into the ultimately stable C–H bond of methane. Additionally, an elegant regulatory mechanism has been defined that enlists size selection and quantum tunneling to allow methane oxidation to occur specifically in the presence of more easily oxidized substrates.

Contents

1. INTRODUCTION

Methanotrophic bacteria exist at the interface of the anaerobic and aerobic worlds, where they can efficiently oxidize the methane (CH_4) derived from anaerobic metabolism as the sole source of carbon and energy (1). The specialized enzyme that makes this possible is methane monooxygenase (MMO). MMO activates O_2 and inserts one atom into an unactivated C–H bond of methane to yield methanol (CH_3OH) without overoxidation:

$$CH_4 + O_2 + NADH + H^+ \rightarrow CH_3OH + H_2O + NAD^+.$$

Methanol is further oxidized in two-electron steps by other pathway enzymes to yield carbon dioxide (CO_2) as well as reduced nicotinamide adenine dinucleotide (NADH) for energy. The CO_2 is largely cycled back into anaerobic metabolism to complete a carbon cycle. The methanotrophs utilize some of the carbon at the oxidation level of formaldehyde for growth (1, 2). Because methane is the only substrate that can be utilized by methanotrophs, it is important that MMO be selective for methane even in the presence of many other more readily oxidized hydrocarbons that can act as adventitious substrates. A study of MMO must then answer two questions: (*a*) What kind of reactive oxygen species is generated in MMO that can break the 105 kcal/mol bond dissociation energy (BDE) bond of methane? (*b*) How does the enzyme use this species to selectively oxidize methane?

Two general types of MMO have been identified. The most common type found in nearly all methanotrophs is a copper-containing, membrane-bound enzyme termed particulate MMO (pMMO) (3). At low copper concentrations, some methanotrophs switch off expression of pMMO and instead synthesize a completely different, iron-containing soluble form (sMMO) (4). sMMO has proven to be easier to purify and study in detail than pMMO. Its favorable characteristics have allowed our research group and others to formulate one of the most complete descriptions of O_2 activation available for any oxidase or oxygenase (5–7). In this review, we endeavor to describe this mechanism and show how it is regulated to ensure specific methane oxidation.

2. sMMO PROTEIN ARCHITECTURE

The studies of sMMO catalysis have been principally focused on enzymes from two bacterial sources, *Methylosinus trichosporium* OB3b (*Mt* OB3b) (5, 6, 8) and *Methylococcus capsulatus* Bath (*Mc* Bath) (7, 9, 10). These bacteria represent two major genera that differ in internal membrane structure and pathway for carbon assimilation, but their sMMOs have proven to be remarkably similar. These studies have shown that sMMO is a multiprotein complex comprising a 245-kDa $(\alpha\beta\gamma)_2$ hydroxylase protein, MMOH; a 16-kDa regulatory protein, MMOB; and a 40-kDa electron transfer reductase, MMOR (8, 9). Multiple crystal structures of MMOH in both the oxidized and reduced states, together with NMR structures of MMOB and the isolated flavin adenine dinucleotide (FAD) and iron sulfur domains of MMOR, have provided a clear picture of the individual protein components as shown in **Figure 1*a–c*** (11–24). The active site is located in MMOH and contains a nonheme diiron cluster coordinated by two histidine (His) and four glutamate (Glu) residues from four α-helices organized in a four-helix bundle motif (5, 11, 12, 14, 25, 26)

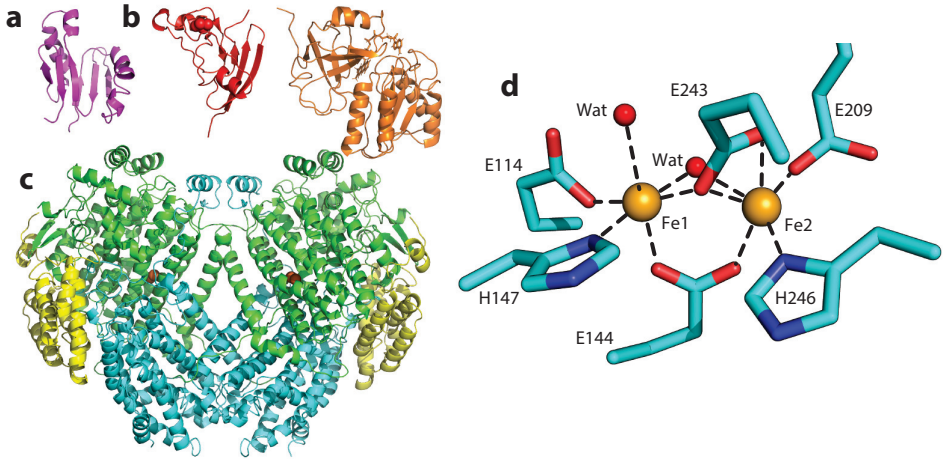

Figure 1

Structures of sMMO components. NMR structures of (*a*) MMOB (*magenta*; PDB: 2MOB or 1CKB), (*b*) the MMOR ferredoxin domain (*red*; PDB: 1JQ4), and the FAD domain (*orange*; PDB: 1TVC). (*c*) X-ray crystal structure of MMOH (PDB: 1MTY or 1MHZ). Each half of MMOH consists of α (*green*), β (*cyan*), and γ (*yellow*) subunits. (*d*) Active site diiron cluster of MMOH. The diferrous state is shown (PDB: 1FYZ). The diferric state (PDB: 1MTY or 1MHZ) is similar, except that glutamate 243 (E243) binds only to Fe2 and an additional solvent bridges the irons. PYMOL (**https://www.pymol.org/**) was used to generate these structural models. Abbreviations: FAD, flavin adenine dinucleotide; MMOB, regulatory component of sMMO; MMOH, hydroxylase component of sMMO; MMOR, reductase component of sMMO; NMR, nuclear magnetic resonance; PDB, Protein Data Bank; sMMO, soluble methane monooxygenase.

(**Figure 1*d***). In the resting state, the iron atoms are ferric (27) and antiferromagnetically coupled through bridging ligands comprising one of the Glu residues (E144) and two hydroxo or aquo groups (5, 11–14). To initiate catalysis, two electrons are required to reduce the diferric cluster ($\mathbf{H^{ox}}$) to the diferrous state ($\mathbf{H^{red}}$) that can subsequently bind O_2 (5, 8, 28). The source of the electrons is NADH-reduced MMOR, which has typical FAD and [2Fe-2S] cofactors (29–32). The cofactorless MMOB component binds to MMOH and serves to regulate entry of O_2, methane, and protons into the active site (5, 8, 30, 33–36).

2.1. The Pore Region of MMOH

In the initial crystal structures of MMOH (11, 14), the diiron cluster appeared to be completely inaccessible to substrates. However, subsequent studies and comparison with other members of the large bacterial multicomponent monooxygenase (BMM) family have revealed potential access routes. One route is via a conserved BMM structural feature known as the pore region (37–39) (**Figure 2*a***). The 12-Å long pore in MMOH extends from the active site pocket directly to the protein surface through two of the α-helices housing the diiron cluster and is the shortest path from bulk solvent to the active site. The MMOH pore region, like those of BMM family counterparts phenylalanine hydroxylase (PHH), toluene/*o*-xylene monooxygenase (ToMO), and toluene 4 monooxygenase (T4MO), is lined with conserved threonine (MMOH T213), asparagine (MMOH N214), and glutamate/glutamine (MMOH E240) residues. In diferric MMOH, E240 and N214 side chains are solvent exposed, whereas T213 side chain faces the active site. On the basis of

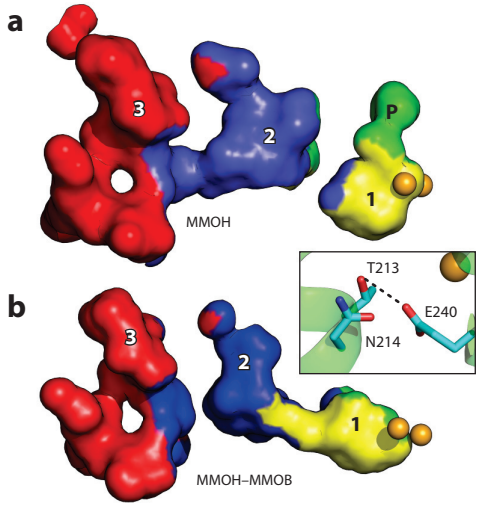

Figure 2

Internal cavities and pore region of MMOH. (*a*) Three cavities and the pore (P) of MMOH alone (PDB: 1MTY). (*b*) Formation of the MMOH–MMOB complex causes connection of cavities 1 and 2 and closing of the pore. This closure is caused by a shift of residues in the pore region and formation of a hydrogen bond between threonine 213 (T213) and glutamate 240 (E240) (*inset*) (PDB: 4GAM). A gap is introduced between cavities 2 and 3, but its significance is unknown. Figure adapted from Reference 36 with permission. PYMOL (**https://www.pymol.org/**) was used to generate these structural models. Abbreviations: MMOB, regulatory component of sMMO; MMOH, hydroxylase component of sMMO; PDB, Protein Data Bank; sMMO, soluble methane monooxygenase.

mutagenesis studies of ToMO (40) and structural comparisons in T4MO (39), it has been proposed that one role for the pore residues is to mediate the transfer of protons from bulk solvent to the diiron center.

2.2. Cavities Within MMOH

A second type of potential access route in the hydroxylase components of many BMM enzymes is a series of three cavities that trace a long 35–40-Å path from the active site to bulk solvent (11, 13, 37–39, 41). In MMOH, the three cavities are located in the α-subunit, and cavity 1 contains the diiron cluster and active site (**Figure 2*a***). It differs from the other BMM enzymes in that the path between cavities 1 and 2 is blocked by residue phenylalanine 188 (F188) (36). The MMOH cavities were characterized by soaking oxidized MMOH crystals with very high concentrations of various halogenated substrate and product analogs and by xenon pressurization experiments (17, 24). Under these conditions, the product analogs were found bound in all three cavities, whereas Xe atoms and substrate analogs were found bound to cavities 2 and 3. Accordingly, the cavities were proposed to serve the dual functions of substrate ingress (CH_4 and O_2) and product egress.

2.3. Conformational Changes in MMOH When MMOB Is Bound

Although MMOH is capable of oxidizing methane slowly in isolation (8), the catalytic ability of MMOH is truly unlocked upon formation of a protein complex with MMOB. Kinetic studies have shown that the turnover number increases by 150-fold, the rate constant for reaction with O_2 increases 1,000-fold, and the product yield doubles (8, 42, 43). The 2.9-Å crystal structure of the protein complex of MMOH with MMOB has provided many insights into how MMOB regulates the catalytic cycle (36) (**Figures 2*b*** and **3*a***). Many structural changes in the α-subunit of MMOH occur, including large-scale movement of secondary structures and rotation of amino acid side chains; 15 out of 19 α-helices and 8 out of 24 loop regions undergo conformational changes, while the β- and γ-subunits remain rigid. The diiron-coordinating ligands shift and rotate, but the distance between the irons and the coordinating ligands is conserved. One exception is E243, where the side chain carboxylate rotates to coordinate with one iron in a bidentate manner and bridges to bind in a monodentate manner to the other iron (**Figure 3*b***). The latter change also occurs in MMOH alone upon reduction (12, 13) (**Figure 1*d***), so the observation in the complex may be due to reduction of MMOH in the synchrotron beam rather than being a direct effect of MMOB binding. The carboxylate shift is important because it is accompanied by the dissociation of one or both solvent bridges between the irons, creating a binding site for O_2 between the irons.

The well-folded core region of MMOB binds directly over the MMOH pore region (**Figure 3*a***). Serine 111 (S111) of MMOB hydrogen bonds to pore residue N214. The T213 side chain shifts slightly and rotates ~180°, while E240 moves ~5 Å, causing the pore to close. The interactions in the pore region are important for regulation, as discussed below (see Section 5). Another consequence of MMOB binding to MMOH is the slight rotation and ~3-Å shift of residue F188. This opens a path between cavities 1 and 2 (**Figure 2*b***), which could potentially facilitate entry of hydrocarbon substrates and O_2 into the active site. Kinetic studies provide a different view of this process, which is discussed below (see Section 5) in the context of regulation.

The nuclear magnetic resonance (NMR) structures of MMOB show a 35-residue disordered region at the N terminus (18–20). Both NMR relaxation measurements and double electron-electron resonance distance measurements using labeled MMOB indicated that this region binds to MMOH in the complex (20, 44). The crystal structure of the complex showed that the MMOB N-terminal sequence forms a ring-shaped structure that lays on the MMOH surface (36)

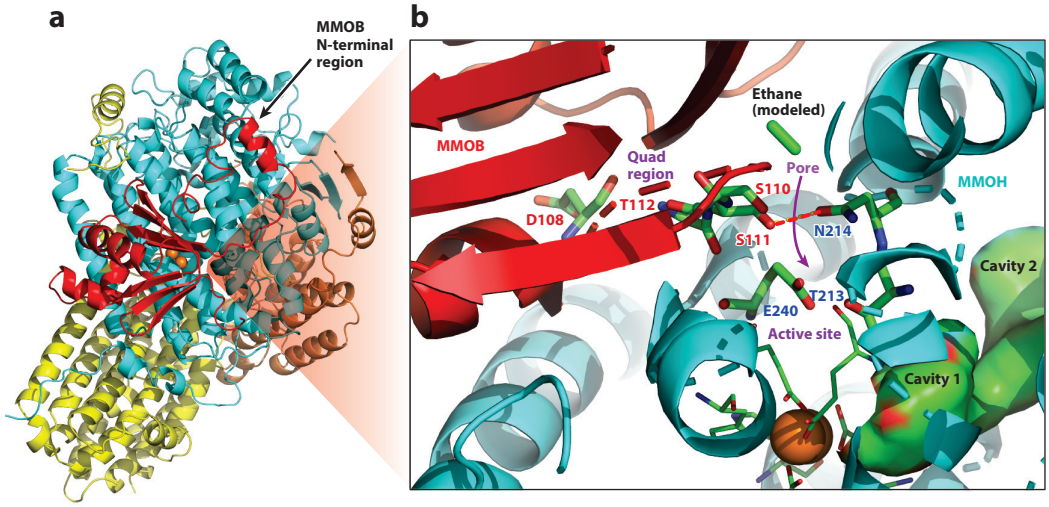

Figure 3

Structure of the *Methylococcus capsulatus* Bath MMOH–MMOB complex. (*a*) MMOB (*red*) binds to the α-subunit of MMOH (*cyan*; PDB: 4GAM). (*b*) The residues replaced in the Quad variant of *Methylosinus trichosporium* OB3b MMOB (*red lettering*; illustrated here using the *Methylococcus capsulatus* Bath MMOB structure and numbering) bind over the pore into the active site of MMOH (residues labeled in *blue lettering*). The Quad variant causes a change in substrate size selection but is remote from cavity 2, which is proposed as an alternative substrate entry route. PYMOL (**https://www.pymol.org/**) was used to generate these structural models. Abbreviations: MMOB, regulatory component of sMMO; MMOH, hydroxylase component of sMMO; PDB, Protein Data Bank; sMMO, soluble methane monooxygenase.

(**Figure 3*a***). Both the N- and C-terminal MMOB regions have major effects on reaction cycle kinetics, as detailed below in Sections 4 and 5 (45, 46).

3. CATALYTIC CYCLE OF sMMO

3.1. Overview

The single-turnover catalytic cycle of sMMO illustrated in **Figure 4** has been studied in detail for the case in which MMOB and MMOH are present and reduction of the diferric MMOH diiron cluster ($\mathbf{H^{ox}}$) is carried out using chemical reductants rather than MMOR and NADH (7, 42, 45, 47–51). The resulting $\mathbf{H^{red}}$–MMOB complex reacts rapidly with O_2 to form intermediate **O** (47). The diiron clusters of $\mathbf{H^{red}}$ and **O** exhibit identical optical and electron paramagnetic resonance (EPR) spectra. The EPR spectra are characterized by a signal at $g = 16$ arising from ferromagnetic coupling of the two high-spin $S = 2$ irons to yield an $S = 4$ species (8, 52). This unique signal proved useful in tracking the kinetics of intermediate **O** conversion through the application of rapid freeze quench (RFQ) techniques (42, 47). The occurrence of **O** was established by the finding that the formation rate constants for all subsequent intermediates in the catalytic cycle are independent of O_2 concentration (43), thereby requiring the irreversible formation of an intermediate between $\mathbf{H^{red}}$ and the downstream intermediates. The lack of spectroscopic change suggests that **O** has O_2 bound in the active site but not to the diiron cluster. In general, the binding and activation of O_2 by the iron atoms occurs through a metal-to-ligand transfer of electrons. Two chromophorically and electronically distinct intermediates (**P*** and **P**) have been characterized in this process, which culminates in the cleavage of the O–O bond to generate the reactive

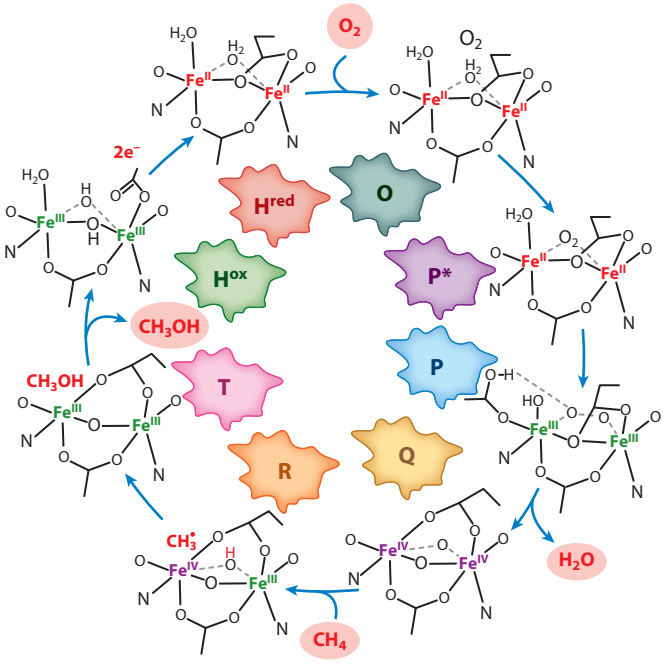

Figure 4

Reaction cycle of sMMO. Only the diiron cluster of MMOH is illustrated. MMOB must be present in equal concentration to the diiron cluster to detect the intermediates. Iron is shown in red, green, and purple in the ferrous, ferric, and Fe^{IV} states, respectively. All of the lettered intermediates except **R** have been directly detected. Rate constants for individual steps in the cycle of the *Methylosinus trichosporium* OB3b are given in References 5, 42, 43, 45, 48, 49, and 51. Figure adapted from References 6, 51, and 59 with permission. Abbreviations: MMOB, regulatory component of sMMO; MMOH, hydroxylase component of sMMO; sMMO, soluble methane monooxygenase. **O**, **H^{red}**, **H^{ox}**, **P**, **P***, **Q**, **R**, **and T** are intermediates of the sMMO reaction cycle in which the MMOH diiron clusters are proposed to have the structures indicated in the figure.

intermediate termed **Q** (42, 48, 50, 51). **Q** can react directly with methane to insert an oxygen atom into one of the C–H bonds. Our proposal for the mechanism (see Section 4) envisioned a hydrogen atom abstraction reaction to yield a cluster-bound hydroxyl radical and a methyl radical species termed **R** (42, 53–55). Subsequent recombination of the radicals would yield the bound methanol product complex **T** (42). Finally, release of methanol from **T** would reform **H^{ox}** in the rate-limiting step of the overall reaction (42). It is interesting to note that in the absence of MMOB, the reaction with O_2 to form either **O** or **P*** becomes the rate-limiting step (43). Thus, the dramatic influence of MMOB on the progress of the reaction was immediately clear from early experiments.

It is important to mention at this point that, unlike most enzyme systems, the rate constants for the steps in the sMMO catalytic cycle decrease as the cycle progresses such that **Q** decays over several seconds in the absence of methane (42). This favorable kinetic scenario enabled the RFQ trapping of the intermediates as they occurred in the single turnover cycle for detailed spectroscopic characterization. Also, even though methane is the only metabolically relevant substrate for sMMO, the enzyme is promiscuous in nature and oxidizes a large range of alternative nonpolar aliphatic and aromatic compounds (5, 9, 49). This catalytic versatility allowed many types of studies to probe the mechanism. The following sections describe the current understanding of the nature of the key reaction cycle intermediates.

3.2. Intermediate P*

Intermediates **O** and **P*** have similar broad, weak absorption spectra in the visible region, with that of **P*** being very slightly more intense between 325 and 700 nm (51). Intermediate **P*** was discovered on the basis of two indirect observations: (*a*) The rate constant for **O** decay monitored at 350 nm or via the decay of its $g = 16$ EPR spectrum (42) is significantly faster than the formation rate constant for intermediate **P** followed at 700 nm, and (*b*) the rate constant for **O** decay is pH independent, whereas that for **P** formation is strongly pH dependent (48, 51). The direct spectroscopic characterization of intermediate **P*** was facilitated by the use of the MMOB mutant H33A (see Section 5), which enhanced the yield of **P*** by decreasing its decay rate constant while leaving its formation rate constant unaffected (45). The observed loss of the $g = 16$ EPR signal during **P*** formation led to the assumption that **P*** would have one or both irons in the ferric state (48, 50). However, RFQ EPR and Mössbauer studies of **P*** showed that it is a diferrous species that does not possess the $g = 16$ signal (51). We proposed that subtle electronic changes in **P*** as O_2 begins the metal binding process cause the loss of the $g = 16$ signal without net oxidation of the diiron cluster. An intermediate between **O** and **P** is also observed in the *Mc* Bath MMOH catalytic cycle (50), but it appears to be a diferric peroxo species similar to **P**.

3.3. Intermediate P

Intermediate **P** ($\mathbf{H_{peroxo}}$ in *Mc* Bath MMOH) has a broad electronic absorption spectrum with a band at 700 nm ($\varepsilon_{700} = 2500\ M^{-1}\ cm^{-1}$) that is characteristic of a peroxo species (48, 50, 51). The Mössbauer spectrum of **P** ($\delta = 0.66$ mm/s, $\Delta E_Q = 1.53$ mm/s) indicates that the iron atoms are present in the ferric oxidation state. Thus, **P** is designated as a diiron(III)-peroxo species. In the absence of a resonance Raman characterization of **P**, the binding mode of the peroxo moiety is an open question. However, a comparison with vibrationally characterized peroxo intermediates in related diiron systems and synthetic model compounds possessing similar spectroscopic features suggests either a *cis*- or *trans*-μ-1,2 binding mode (7, 26). A comparison of the Mössbauer isomer shift with those of protonated and deprotonated peroxo intermediates in synthetic model compounds of mononuclear Fe^{III}–peroxo complexes suggests that the deprotonated peroxo ligand is present in **P** (51). However, no model complexes for protonated diiron complexes have yet been synthesized. A reaction of **P** with hydrocarbon substrates has not been observed (42), although reaction with easily oxidized substrates has been described (56, 57).

The rate constants for both formation and decay of **P** were found to increase with a decrease in pH from 8.5 to 6.5 (48, 50). Proton inventory studies in which H_2O is progressively replaced with D_2O in the buffer showed that a single proton is involved in each step in a one-hop process from a donor group with a fractionation factor near 1 and a pK_a value of 7.6 (48). A water molecule bound to one of the iron atoms, as seen consistently in crystal structures, is believed to be the most likely source of the proton (48). If the peroxo-bridge in **P** is unprotonated, the proton transfer could possibly be to the carboxylate function of one of the Glu ligands to the diiron cluster. Such a transfer is supported by studies with synthetic diiron model compound mimics of **P** (58).

3.4. Intermediates Q and T

The rate constant for formation of **Q** is independent of substrate concentration, but the decay rate constant exhibits a linear dependence for most substrates (42). In contrast to the preceding intermediates in the reaction cycle, intermediate **Q** possesses an intense electronic absorption spectrum with bands at 330 and 430 nm ($\varepsilon_{330} = 9800\ M^{-1}\ cm^{-1}$, $\varepsilon_{430} = 7500\ M^{-1}\ cm^{-1}$)

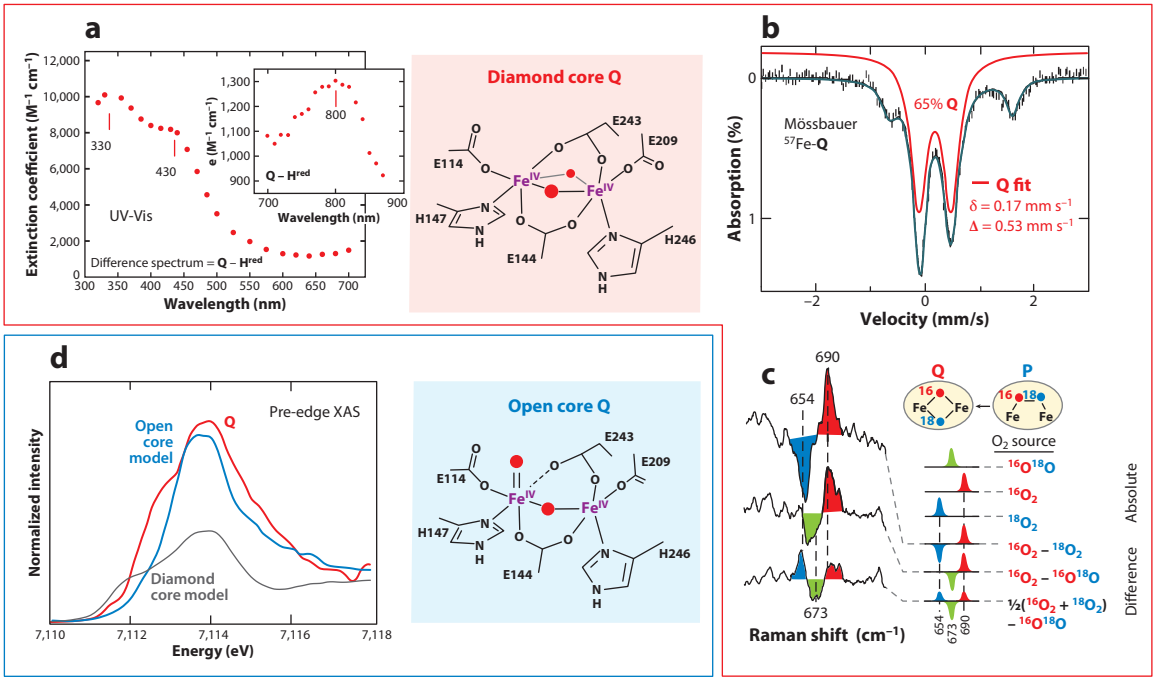

Figure 5

Two proposed structures for intermediate **Q**. Experimental evidence favoring a diamond core **Q** includes the following: (*a*) UV-Vis features at 330, 430, and 800 nm with high-extinction coefficients characteristic of diamond core model complexes; (*b*) a single Mössbauer quadrupole double showing that the irons are in similar environments, which is inconsistent with the single $Fe^{IV} = O$ of the open core structure; and (*c*) a resonance Raman feature at 690 cm^{-1} with the isotopic shifts characteristic of diamond core tetra-atomic vibration. Panels *a* and *c* adapted from Reference 59 with permission. Experimental evidence favoring an open core **Q** includes (*d*) pre-edge XAS intensity and EXAFS spectra (67) similar to those of an open core model. Panel *d* adapted from Reference 66 with permission. The high reactivity of **Q** is also characteristic of the open core in model complexes. Abbreviations: EXAFS, extended X-ray absorption fine structure; MMOB, regulatory component of sMMO; MMOH, hydroxylase component of sMMO; sMMO, soluble methane monooxygenase; UV-Vis, ultraviolet-visible spectroscopy; XAS, X-ray absorption spectroscopy. $\mathbf{H^{red}}$, **P**, and **Q** are intermediates of the sMMO reaction cycle with the diiron cluster of MMOH in the diferrous, peroxo, and dinuclear Fe^{IV} reactive states, respectively.

(42, 59) (**Figure 5*a***). The Mössbauer spectrum of **Q** in *Mt* OB3b MMOH indicates the presence of two antiferromagnetically coupled high-spin Fe^{IV} atoms in similar electronic environments ($\delta = 0.17$ mm/s, $\Delta E_Q = 0.53$ mm/s) (60) (**Figure 5*b***). To date, this is the only characterized biological example of a dinuclear Fe^{IV} cluster. The irons in *Mc* Bath sMMO **Q** are also both Fe^{IV}, but Mössbauer studies show they reside in slightly dissimilar electronic environments (47, 61).

The time-resolved resonance Raman spectrum of **Q** (**Figure 5*c***) exhibits an Fe–O vibrational mode at 690 cm^{-1} when generated with $^{16}O_2$ that downshifts to 654 cm^{-1} when made with $^{18}O_2$ (59). Upon the formation of **Q** with the mixed-label O_2 isotope $^{16}O^{18}O$, an intermediate vibrational mode is observed at 673 cm^{-1}. A comparison with the vibrational spectra of model complexes shows that the frequencies and isotopic shifts for **Q** match those of the tetra-atomic vibration of an Fe_2-(μ-O)$_2$ diamond core structure (62) (illustrated in **Figure 5*c***). The $^{16}O^{18}O$ labeling pattern also indicates that both oxygen atoms from O_2 are retained in the diamond core upon conversion from intermediate **P** to **Q**, an observation that lends support to a homolytic cleavage model of the O–O bond. Upon reaction of **Q** with methane, one of the oxygen atoms is transferred to the methanol product (63). A new vibrational mode at 556 cm^{-1} that downshifts to 533 cm^{-1}

for samples prepared with $^{18}O_2$ was observed (59), showing that the second atom of oxygen from O_2 is retained in the mono-μ-oxo-bridged diferric cluster of the product complex **T**.

An early Mössbauer and extended X-ray absorption fine structure (EXAFS) investigation of **Q** provided the first indication that it might have a diamond core structure. The two Fe^{IV} atoms were found to be 2.46 Å apart, and each iron was found to have Fe–O bonds of 1.77 Å and 2.05 Å that could not be assigned to protein ligands (64). The Fe–O bonds are too long to be assigned as an $Fe^{IV} = O$ moiety on the basis of model compounds (65). The most reasonable structure to account for these characteristics is the diamond core. In the last two decades since the EXAFS study of **Q**, a large range of synthetic model compound mimics of **Q** have been generated (26). Improvements to the X-ray absorption spectroscopy (XAS) techniques, such as Fe Kα high-energy-resolution fluorescence-detected XAS (HERFD XAS), have also enhanced the resolution of the pre-edge XAS features. A recent study employed both of these advances along with time-dependent density functional theory calculations to study the pre-edge XAS spectrum of **Q** (66) (**Figure 5*d***). The pre-edge intensity of **Q** was observed to be three times higher than those of a diamond core model complex but comparable with that of an open-core model complex containing a terminal $Fe^{IV} = O$ and a mono-μ-oxo-bridging moiety (illustrated in **Figure 5*d***). A recent reinvestigation of the early EXAFS study utilizing HERFD methods favored a much longer Fe-Fe distance, also consistent with the open-core structure for **Q** (67).

The open core model for **Q** finds support from the observation that open-core and diamond core model compounds with the same ligand environment exhibit vastly different oxidizing reactivity (68). The open-core species with a terminal oxo moiety was found to be 1,000 times more reactive than the diamond core model (after spin state compensation). It is important to add the caveat that a diamond core model complex with high-spin iron ($S = 2$) atoms like those of **Q** has not yet been generated (26). Nonetheless, both the XAS and model studies suggest a role for a terminal $Fe^{IV} = O$ moiety in the reaction with methane. One possibility is that **Q** may exist in an equilibrium between open-core and diamond core structures in which the more potent open-core structure can react with methane.

4. CHEMICAL MECHANISM OF sMMO

The remarkable ability of sMMO to catalyze one of the most difficult oxidation reactions in organic chemistry at room temperature and halt after a single oxygen transfer has encouraged many experimental and computational attempts to understand the mechanism. The computational studies have all been based on the same X-ray crystal structures of $\mathbf{H}^{ox}$ and $\mathbf{H}^{red}$, but differences in the size of the adopted active site model and the specific method employed [e.g., choice of density function theory (DFT) functional or hybrid quantum mechanics/molecular mechanics (QM/MM) approaches] have resulted in significantly different proposed mechanisms. Generally, the mechanisms for the C–H bond breaking and oxygen insertion reactions fall into the traditional concerted or nonconcerted classes (69–74). The experimental results are readily accounted for by the nonconcerted models. However, it has been shown that the concerted mechanisms can also account for the experimental observations under special conditions [e.g., formation of an Fe–C bond that causes distortion of the tetrahedral symmetry of the substrate carbon (75, 76), asynchrony of vibrational modes in the bond-breaking and bond-forming reactions in the transition state (77), or coordinated electrophilic and nucleophilic attack by two $Fe^{IV} = O$ moieties leading to the formation of a pentavalent carbon intermediate (78)]. Whether these special conditions are possible in a biological system is unclear. The most recent computations have utilized a large model and employed molecular mechanic methods to assess the role of the protein beyond the first sphere of the metals (79). These models favor a hydrogen atom abstraction reaction.

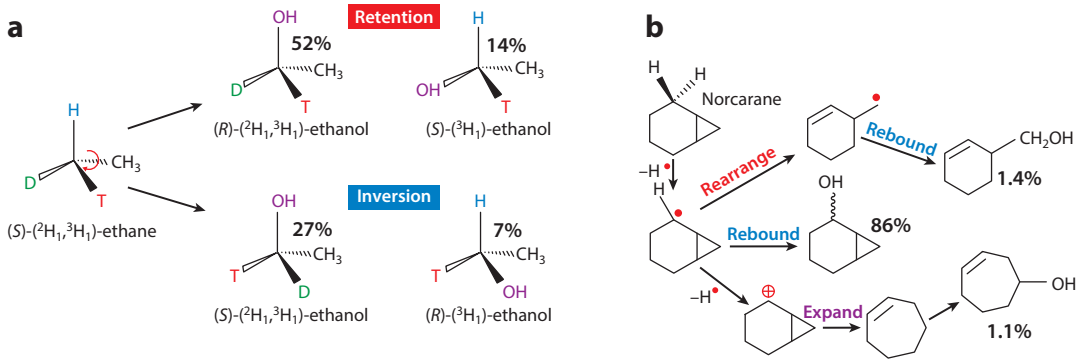

Figure 6

Examples of experimental evidence for radical or cation intermediates. (*a*) Chiral ethane is converted to chiral ethanol with 34% inversion of stereochemistry by soluble methane monooxygenase (sMMO), implying an intermediate with a lifetime <1 ps. (*b*) Products from the norcarane reaction with sMMO show primarily radical (lifetime <20 ps) but also cation intermediates.

4.1. Key Insights into the Mechanism from Chiral Substrate Reactions

The chemical mechanism of cytochrome P450 oxygenase was proposed by our group and others as a model for sMMO catalysis (8, 9, 80). This mechanism involves abstraction of a hydrogen atom from the substrate by the heme $Fe^{IV} = O$ π cation radical reactive species to give a substrate radical and heme Fe^{IV}–OH (81, 82). Rebound of the hydroxyl radical to the substrate radical completes the hydroxylation reaction. The **Q** intermediate of sMMO is electronically equivalent to the heme $Fe^{IV} = O$ π cation radical and might be expected to carry out similar chemistry. The direct detection of a transient substrate radical intermediate is almost impossible, considering the ultrashort lifetimes expected for such species when the reactive hydroxyl radical associated with the diiron cluster is nearby in the active site. One type of indirect detection employed the use of chiral hydrocarbon substrates (**Figure 6*a***). The *Mt* OB3b sMMO catalyzed oxidation of chiral, carrier-free (*R*) and (*S*) [1-$^2H_1$, 1-$^3H_1$] ethane to ethanol proceeded with 34% inversion of stereochemistry (53). Likewise, the chiral ethane and chiral butane hydroxylation reactions with *Mc* Bath sMMO displayed a 28% and 23% inversion of stereochemistry, respectively (83). These results are consistent with formation of a radical or cation intermediate, but the lack of complete racemization suggests a very short lifetime on the order of a C–C bond rotation ($k = 10^{12}$ to 10^{13} s^{-1}). This rate constant is too fast for a physical motion of the hydroxyl group as it rebounds onto the substrate radical, indicating that hydroxylation in sMMO is subtly different from a classical two-step radical mechanism attributed to P450. A computational model assuming a caged structure that locks the radical species in close proximity provides a reasonable explanation for these observations (79, 84, 85).

4.2. Radical Clock Reactions

A large variety of radical clock compounds have been used as sMMO substrates to assess the presence of transient radical intermediates (54, 55, 86–88) (see **Figure 6*b*** for one example). In summary, rearranged products derived from both radical and cation substrate intermediates have been observed for several of these substrates. However, the lack of correlation between rearranged product yield and rearrangement rates for the radical clocks suggests that steric factors in the active site alter how radical clock substrates are presented to **Q**. The role of steric factors in the oxidation reaction agrees with earlier experiments probing the stereochemistry of isopentane

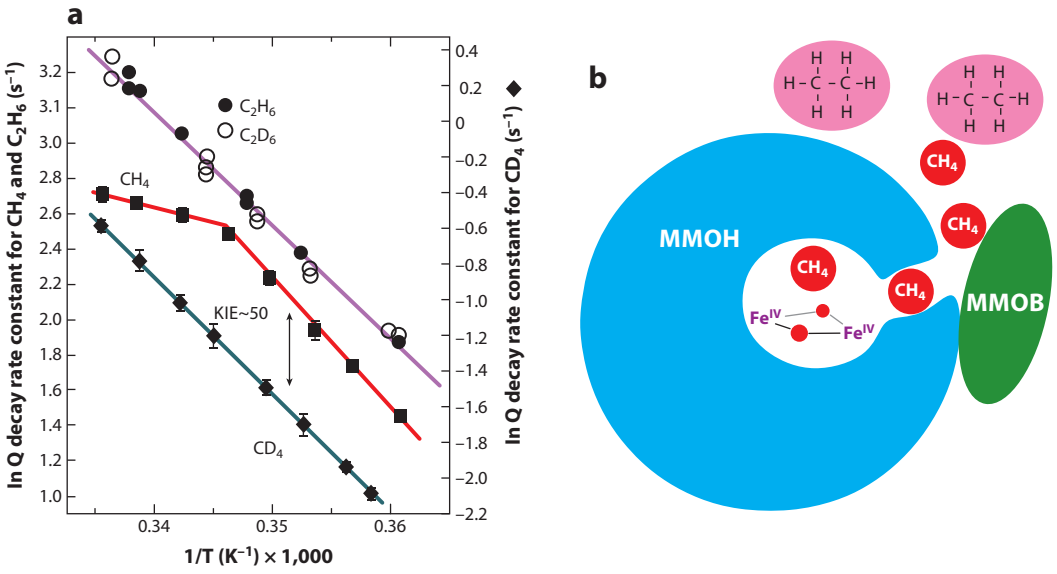

Figure 7

(*a*) Arrhenius plots for intermediate **Q** reaction with substrates. The large KIE for methane reaction with **Q** and the lack of a KIE for the reaction with ethane are illustrated. Only the Arrhenius plot for the methane reaction exhibits a break due to a change in the rate-limiting step in the accessible temperature range. Substrate concentration = 400 μM. (*b*) The molecular sieve model. Panel *a* adapted from References 6 and 49 with permission. Abbreviations: KIE, kinetic isotope effect; MMOB, regulatory component of sMMO; MMOH, hydroxylase component of sMMO; sMMO, soluble methane monooxygenase.

oxidation, where it was observed that the least sterically hindered carbon atom of isopentane was preferentially hydroxylated despite its stronger C–H bonds (34). Although radical clock sMMO substrates can be used only qualitatively, they do indicate in all cases that the radical lifetimes are very short ($k_{rebound} > 10^{10}$ s^{-1}), consistent with the results of the chiral substrate experiments.

4.3. Isotope Effect Studies

The chromophore of **Q** allows the reaction with substrates to be directly observed. We are aware of no other case for a biological system in which the specific oxygen transfer step can be studied independently of other steps in the reaction cycle. One application of this experimental advantage was the direct determination of the intermolecular deuterium kinetic isotope effect (KIE) on the rate constant of the **Q** reaction with methane (**Figure 7*a***). The KIE value of 50 for this reaction is one of the largest for any biological system (63, 89, 90). A KIE value of this order unequivocally indicates the C–H bond-breaking step is the primary determinant in the reaction coordinate of methane oxidation by **Q**. Remarkably, hydrocarbon substrates with a molecular size larger than methane failed to display a KIE (90). This interesting result is discussed in Section 5. As in the case of the chiral substrate and radical clock experiments, the observation of a large KIE is clearly supportive of a nonconcerted mechanism.

4.4. Quantum Tunneling in the sMMO Reaction

The primary intermolecular deuterium KIE for methane reaction with **Q** far exceeds the classical limit of approximately 7, suggesting the presence of a hydrogen atom tunneling contribution in the C–H bond-breaking reaction. A definitive proof of hydrogen tunneling requires kinetic studies

over a much larger temperature range than is possible with sMMO (91). However, a plot of natural log KIE versus 1/T in the temperature range in which C–H bond breaking is rate limiting shows a positive slope of 3.4, which is larger than an expected value of 1.25 based upon a difference in the zero point bond-dissociation energy for the isotopes (92). This value is similar to those obtained from other enzymes demonstrated to exhibit tunneling (93), thereby supporting a role for tunneling in the reaction of **Q** with methane (94).

5. REGULATION OF sMMO

Oxygenases in general, and sMMO in particular, must employ mechanisms to ensure that the powerful reactive species they generate react with substrates with high specificity. A second regulatory consideration for monooxygenases is the requirement to couple reducing equivalents utilized to initiate O_2 activation with substrate oxygenation. The most common form of regulation in oxygenases involves the initiation of the catalytic cycle solely in the presence of substrate, but many other strategies have been described (95–102). Regulation in sMMO plays out at many different stages during the catalytic cycle. However, regulation by substrate triggering of oxygen activation does not appear to be utilized, because none of the rate constants through **Q** formation are affected by the presence of hydrocarbon substrates (42). sMMO must be capable of overcoming two major regulatory hurdles. First, all of the alternative substrates of sMMO are easier to oxidize than methane but metabolically useless to a methanotroph, so a mechanism to favor methane oxidation must be present. Second, the enzyme must have a mechanism to prevent MMOR from reducing **Q** before it can react with methane. The effector protein MMOB appears to play a pivotal role in overcoming these hurdles.

5.1. Role of MMOB in Controlling O_2 Binding to the Diiron Cluster

MMOB greatly accelerates the first steps of the reaction cycle leading ultimately to **Q** formation. Some insight into the mechanism by which this change occurs has been provided by circular dichroism (CD), magnetic circular dichroism (MCD), and variable temperature variable magnetic field (VTVH) MCD spectroscopies and ligand field (LF) and DFT calculations (103, 104). These studies showed that the binding of MMOB caused two types of structural changes in $\mathbf{H}^{red}$. CD indicated a global change in the diiron cluster environment, whereas MCD and VTVH MCD also showed a local change at one of the irons. In contrast, MMOB variants that did not accelerate the O_2 binding steps caused only the MCD and VTVH MCD changes, showing that global change in sMMOH structure detected by CD is also required for full activity. The possible significance of this global structural change is discussed in Section 5.2.

5.2. Role of MMOB in Gating Methane Substrate Entry into MMOH

The unexpected linear change in the rate constant of **Q** decay with substrate concentration (42, 89) has at least two reasonable explanations. Either the reaction is truly second order, in which collision of activated MMOH with the substrate results in immediate oxygen transfer, or the collision results in slow complex formation followed by very rapid reaction with **Q**. One approach used to distinguish these possibilities was to determine the rate constant of **Q** decay as a function of temperature. Typically, the Arrhenius plots from such an experiment are linear, as observed for fully deuterated methane and all substrates other than methane (**Figure 7*a***). In contrast, the use of methane as the substrate causes the plot to display a discrete break point (49). It was proposed that the nonlinear Arrhenius plots indicated the presence of two chemical steps in the decay of **Q** with

methane: nominally substrate binding followed by reaction with **Q**. If the activation parameters for these two steps are different, then the rate-limiting step might change in the temperature range of the experiment. Fully deuterated methane has a much stronger C–H than methane and exhibits a slower reaction with **Q** (63), so its bond-breaking reaction might be rate limiting throughout the observable temperature range. Conversely, if substrates larger than methane bind slowly, binding might be rate limiting at all accessible temperatures. This scenario would lead to the prediction that substrates larger than methane would not exhibit a KIE for the reaction with **Q**, as observed (**Figure 7*a***). The combination of size-restricted binding and very fast reaction with **Q** due to weaker C–H bonds means that the observed rate constants for all substrates other than methane do not reflect the BDE of the bond. Thus, the comparatively fast rate constant for methane reaction is reflective of its size rather than its stability. Returning to the two possible explanations for the linear change in the rate constant of **Q** decay with substrate concentration cited above, the methane reaction is effectively collisional, whereas the reactions of larger substrates are best described by slow binding followed by rapid reaction with **Q**. We termed this regulatory mechanism the molecular sieve effect (**Figure 7*b***) of MMOH to suggest that something in its structure is size selective for molecules the size of methane (45).

The molecular sieve effect was investigated further using MMOB variants. The interface between MMOB and MMOH was first identified by cross-linking and spectroscopic studies (18–20, 30, 32, 35, 105, 106) and then confirmed by the X-ray crystal structure of the MMOH–MMOB complex (36). The biophysical studies allowed the selection of four key MMOB residues in the center of the interface. These residues were changed to smaller residues in MMOB from *Mt* OB3b to form the Quad variant (N107G/S109A/S110A/T111A) (**Figure 3*b*** shows this region for the *Mc* Bath MMOB–MMOH complex). Analysis of the reaction cycle kinetics in the presence of this variant showed the following perturbations: (*a*) a substantial increase in the rate constant of reaction of **Q** with large substrates like nitrobenzene and furan, (*b*) faster release of products from large substrates from the active site, and (*c*) a decrease in the rate constant of **Q** reaction with methane (**Figure 8*a***) (45, 107). The enhancement in the decay rate constant of **Q** and accelerated product release observed for large substrates was interpreted to suggest that the smaller residues in the MMOH–MMOB interface effectively increase the pore size of the molecular sieve. Another method to validate the molecular sieve hypothesis was to show that increasing access to larger substrates using the Quad variant would make C–H bond cleavage rate limiting and allow a KIE to be detected. Accordingly, a KIE of 2.0 was observed for ethane (90). The location of the putative molecular sieve pore is unknown; however, the well-characterized MMOH pore region immediately over the active site where the Quad variant binds would be a good candidate, as illustrated in **Figure 3*b***.

A competing proposal for a route of methane (and perhaps O_2) entry into the MMOH active site invokes the series of interconnected hydrophobic cavities in MMOH described above (108) (**Figure 2**). In support of this proposal, mutagenesis and kinetic studies with the related ToMO enzyme suggested that O_2 enters the active site using an analogous route (109). However, the series of cavities in MMOH is 35–40 Å long and would likely fill with methane as it does with halogenated alkanes and xenon in the crystallographic experiments that were used to demonstrate its existence. If this is the case, methane would be delivered to **Q** from a bound state in the channel rather than from solution, so the rate constant for the reaction would not appear to be linear with methane concentration.

The linear substrate concentration dependence suggests that no matter how substrate binding is regulated, a structural change must occur when **Q** is formed to permit substrate entry from bulk solvent. In this context, the observation that the pore is closed in the oxidized (and likely reduced) MMOB–MMOH complex (**Figure 2*b***) is in accord with the kinetic data. The competing models

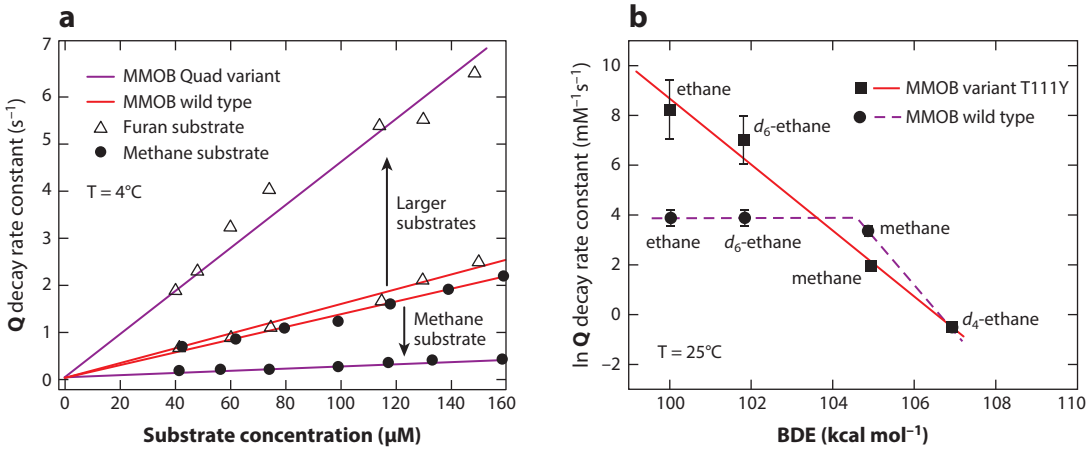

Figure 8

Regulatory effects of MMOB revealed by variants. (*a*) Linear substrate concentration dependence of the **Q** decay rate constant. The Quad variant of *Mt* OB3b MMOB increases the second-order rate constant for larger substrates by opening the molecular sieve and decreases that for the methane reaction owing to loss of tunneling. Panel *a* adapted from Reference 45 with permission. (*b*) The T111Y variant of *Mt* OB3b appears to open the active site, removing the molecular sieve effect and tunneling. Accordingly, the rate constants for methane and ethane reaction with **Q** reflect the C–H BDE of the molecules. Panel *b* adapted from Reference 107 with permission. Abbreviations: BDE, bond dissociation energy; MMOB, regulatory component of soluble methane monooxygenase (sMMO); *Mt* OB3b, *Methylosinus trichosporium* OB3b.

for regulation of substrate binding could, in principle, be tested by making MMOH variants. Unfortunately, heterologous expression of MMOH has not been successful despite the sustained efforts of many research groups. Promising approaches using homologous expression have been reported (110–112).

5.3. Role of MMOB in Regulating Quantum Tunneling in Methane Oxidation

Quantum tunneling plays a major role in methane but not ethane oxygenation, as evidenced by the ethane KIE in the classical range even when the molecular sieve is opened using the Quad variant (90). Importantly, the KIE for methane is decreased from the tunneling range of 50 to the classical range of 6 when this variant is used, suggesting that tunneling has been compromised. Thus, the conformational changes caused by MMOB in the MMOH–MMOB complex not only open the active site for methane but also direct the approach of methane to the diiron cluster to optimize the orbital overlap required for tunneling (113). The same precise MMOH active site structural changes apparently do not occur when the MMOB–MMOH interface is perturbed by the use of MMOB variants, as indicated by the lack of CD spectral change noted above (103). When wild-type MMOB is used, ethane is not granted easy access, and once in the active site, its oxygenation does not occur preferentially by tunneling. Together, these effects account for the ~4,000-fold rate advantage given to methane over ethane on the basis of their roughly equal rate constants of reaction with **Q** despite a 5 kcal/mol difference in BDE. One way to test this proposal arose from the finding that the T111Y variant of MMOB appeared to interact with MMOH in a way that opened the active site completely, thereby removing both the sizing and tunneling advantages given to methane (107). The natural log k_{obs} versus BDE plot shown in **Figure 8*b*** for normal and deuterated methane and ethane was found to be linear and also demonstrated the expected differences in rate constant due purely to the strength of the hydrocarbon bonds.

5.4. Regulation by the N-Terminal and C-Terminal Regions of MMOB

There are regions other than the well-folded core of MMOB where mutations alter the rate constants of chemical steps at the MMOH diiron cluster. For example, deletion of the first 29–35 residues of the N-terminal region of MMOB abolishes steady-state activity (20, 36, 114). Among the substitution mutants, the H33A and H5A MMOB variants decrease the rate constant of conversion of **P*** to **P** and **P** to **Q**, respectively (45). This effect might be attributed to a role for histidine in providing the protons required for these steps. However, the proton inventory plots for these steps are not compatible with multistep transfer of the protons, which would be required from surface histidines. Alternatively, a loss of ability to effect a structural change at the diiron cluster by the H33A and H5A variants could be responsible for the slow formation of **P** and **Q**.

The C-terminal region of MMOB is also implicated in the regulation of kinetic steps in the catalytic cycle. Deletion mutants decreased the rate constant of formation of intermediate **P** and lowered the steady-state turnover number associated with **T** decay (46). Moreover, these variants resulted in a large uncoupling of the reaction due to a dissociation of peroxide from **P**. Thus, the regulatory role of MMOB extends to ensuring a properly coupled turnover system to maximize product yield and prevent the generation of toxic reactive oxygen species.

5.5. Continuous Binding of MMOB During Catalysis

Interestingly, when all of the MMOB variants tested to date are considered together, at least one can be found that alters the rate constant for each step in the catalytic cycle (45, 107). One application of these variants has been to test whether MMOB dissociates from MMOH during the reaction cycle. When the reaction was initiated in the presence of two MMOB variants that affect the rate constants of different steps, the time course of the reaction could be simulated only under the assumption that no MMOB dissociation of either variant occurred between O_2 binding and product release (45).

5.6. Roles of MMOB in the Regulation of Electron Transfer to the Diiron Cluster

The presence of reduced MMOR during single turnover reactions significantly lowers product yield unless MMOB is also present (31). This observation suggests that MMOB plays a role in preventing the transfer of electrons to **Q** from MMOR. One way in which this might be implemented is if the MMOH–MMOB complex at the **Q** stage of the reaction cycle blocks formation of the MMOH–MMOR complex. Conflicting results remain over whether MMOB and MMOR compete with each other for binding MMOH at any stage of the cycle (115, 116). However, early chemical cross-linking studies showed that a ternary MMOH–MMOB–MMOR protein complex can form and that MMOR and MMOB cross-link preferentially to different MMOH subunits (30). Recent hydrogen–deuterium exchange coupled to mass spectrometry experiments showed that the MMOR–MMOH interface in the *Mc* Bath sMMO system overlaps with the MMOB–MMOH binding surface (116). Taking all of these findings into account, a model has emerged in which reduced MMOR binds diferric MMOH in place of MMOB and reduces the diiron cluster (116). MMOB then displaces MMOR from the pore region of MMOH, whereupon the catalytic cycle starts with O_2 binding. The finding described in Section 5.5 that MMOB remains bound throughout the remainder of the cycle explains why MMOR does not rebind to quench **Q** by electron transfer. One potential problem with this scenario is that the affinity of MMOB for *Mt* OB3b MMOH in the diferric state is very high (68 nM) and decreases at least three orders of magnitude when MMOH is reduced (105). These values were directly measured by fluorescence titration of

MMOB labeled with a fluorophore, but they are also in accord with the 132-mV decrease in the redox potential of MMOH when the complex with MMOB is formed (117). The high affinity of MMOB for *Mc* Bath MMOH was not observed (44), but a similar shift in redox potential, which requires a large decrease in affinity, was reported (118). Consequently, for regulation by component displacement proposal to be correct, the affinity of reduced MMOR to $\mathbf{H^{ox}}$ must be even higher than that of MMOB, and the opposite must be true for oxidized MMOR binding to $\mathbf{H^{red}}$. The observed shift in redox potential coupled to binding for formation of the MMOH–MMOR complex does not support this model for MMOR binding (31). However, the hysteretic effects of MMOR on the MMOH redox potential make the shift difficult to measure (31, 119).

6. SUMMARY AND FUTURE DIRECTIONS

The studies of sMMO over the past four decades have generated a unified view of this remarkable enzyme system on most fronts. Specifically, the central role of the dinuclear iron cluster, the step-by-step building of the reactive dinuclear Fe^{IV} species **Q**, and the many modes of regulation by MMOB are widely accepted. Some controversy remains regarding the mechanism of **Q** reaction owing to the many computational studies that have emerged. However, the experimental evidence available is consistent in supporting a hydrogen atom abstraction mechanism akin to that of heme P450 for this nonheme enzyme. The mode of entry of substrates into the active site remains under debate and must await a breakthrough in the heterologous expression of MMOH. Ongoing studies of the exact structure of **Q** are likely to soon yield a consensus view, although more studies will be required to evaluate the possibility that **Q** may have an observable quasi-stable form as well as a reactive form that can break the C–H bond of methane. The studies of sMMO have been tightly integrated with research leading to the synthesis of inorganic model complexes (26, 120). Some of these diiron cluster-containing models can now mimic the high valent irons and high reactivity of **Q**, although reaction with methane has not been achieved. Future applications of these models in chemical feedstock and fuel conversions seem likely (121). The direct use of sMMO has been achieved in bioremediation, but the absence of a heterologous expression system and the scale of manufacturing and biofuel applications have proven to be significant obstacles to success. Nevertheless, sMMO **Q** remains Nature's most powerful biological oxidant, with many lessons in catalysis remaining undiscovered.

DISCLOSURE STATEMENT

The authors are not aware of any affiliations, memberships, funding, or financial holdings that might be perceived as affecting the objectivity of this review.

ACKNOWLEDGMENTS

This work has been supported in the authors' laboratory by National Institutes of Health grants GM40466, GM100943, and GM118030 to J.D.L. and GM008347 to J.C.J.

LITERATURE CITED

1. Hanson RS, Hanson TE. 1996. Methanotrophic bacteria. *Microbiol. Rev.* 60:439–47
2. Chistoserdova L, Gomelsky L, Vorholt JA, Gomelsky M, Tsygankov YD, Lidstrom ME. 2000. Analysis of two formaldehyde oxidation pathways in *Methylobacillus flagellatus* KT, a ribulose monophosphate cycle methylotroph. *Microbiology* 146:233–38
3. Sirajuddin S, Rosenzweig AC. 2015. Enzymatic oxidation of methane. *Biochemistry* 54:2283–94

4. Colby J, Stirling DI, Dalton H. 1977. The soluble methane monooxygenase of *Methylococcus capsulatus* (Bath): Its ability to oxygenate *n*-alkanes, *n*-alkenes, ethers, and alicyclic, aromatic, and heterocyclic compounds. *Biochem. J.* 165:395–402
5. Wallar BJ, Lipscomb JD. 1996. Dioxygen activation by enzymes containing binuclear non-heme iron clusters. *Chem. Rev.* 96:2625–57
6. Banerjee R, Komor AJ, Lipscomb JD. 2017. Use of isotopes and isotope effects for investigations of diiron oxygenase mechanisms. *Meth. Enzymol.* 596:239–90
7. Tinberg CE, Lippard SJ. 2011. Dioxygen activation in soluble methane monooxygenase. *Acc. Chem. Res.* 44:280–88
8. Fox BG, Froland WA, Dege JE, Lipscomb JD. 1989. Methane monooxygenase from *Methylosinus trichosporium* OB3b. Purification and properties of a three-component system with high specific activity from a type II methanotroph. *J. Biol. Chem.* 264:10023–33
9. Pilkington SJ, Dalton H. 1990. Soluble methane monooxygenase from *Methylococcus capsulatus* (Bath). *Methods Enzymol.* 188:181–90
10. Baik M-H, Newcomb M, Friesner RA, Lippard SJ. 2003. Mechanistic studies on the hydroxylation of methane by methane monooxygenase. *Chem. Rev.* 103:2385–419
11. Rosenzweig AC, Frederick CA, Lippard SJ, Nordlund P. 1993. Crystal structure of a bacterial non-haem iron hydroxylase that catalyses the biological oxidation of methane. *Nature* 366:537–43
12. Rosenzweig AC, Nordlund P, Takahara PM, Frederick CA, Lippard SJ. 1995. Geometry of the soluble methane monooxygenase catalytic diiron center in two oxidation states. *Chem. Biol.* 2:409–18
13. Rosenzweig AC, Brandstetter H, Whittington DA, Nordlund P, Lippard SJ, Frederick CA. 1997. Crystal structures of the methane monooxygenase hydroxylase from *Methylococcus capsulatus* (Bath): implications for substrate gating and component interactions. *Proteins* 29:141–52
14. Elango N, Radhakrishnan R, Froland WA, Wallar BJ, Earhart CA, et al. 1997. Crystal structure of the hydroxylase component of methane monooxygenase from *Methylosinus trichosporium* OB3b. *Protein Sci.* 6:556–68
15. Whittington DA, Lippard SJ. 2001. Crystal structures of the soluble methane monooxygenase hydroxylase from *Methylococcus capsulatus* (Bath) demonstrating geometrical variability at the dinuclear iron active site. *J. Am. Chem. Soc.* 123:827–38
16. Whittington DA, Sazinsky MH, Lippard SJ. 2001. X-ray crystal structure of alcohol products bound at the active site of soluble methane monooxygenase hydroxylase. *J. Am. Chem. Soc.* 123:1794–95
17. Whittington DA, Rosenzweig AC, Frederick CA, Lippard SJ. 2001. Xenon and halogenated alkanes track putative substrate binding cavities in the soluble methane monooxygenase hydroxylase. *Biochemistry* 40:3476–82
18. Chang SL, Wallar BJ, Lipscomb JD, Mayo KH. 1999. Solution structure of component B from methane monooxygenase derived through heteronuclear NMR and molecular modeling. *Biochemistry* 38:5799–812
19. Walters KJ, Gassner GT, Lippard SJ, Wagner G. 1999. Structure of the soluble methane monooxygenase regulatory protein B. *PNAS* 96:7877–82
20. Chang SL, Wallar BJ, Lipscomb JD, Mayo KH. 2001. Residues in *Methylosinus trichosporium* OB3b methane monooxygenase component B involved in molecular interactions with reduced- and oxidized-hydroxylase component: a role for the N-terminus. *Biochemistry* 40:9539–51
21. Muller J, Lugovskoy AA, Wagner G, Lippard SJ. 2002. NMR structure of the [2Fe-2S] ferredoxin domain from soluble methane monooxygenase reductase and interaction with its hydroxylase. *Biochemistry* 41:42–51
22. Chatwood LL, Mueller J, Gross JD, Wagner G, Lippard SJ. 2004. NMR structure of the flavin domain from soluble methane monooxygenase reductase from *Methylococcus capsulatus* (Bath). *Biochemistry* 43:11983–91
23. Sazinsky MH, Merkx M, Cadieux E, Tang S, Lippard SJ. 2004. Preparation and X-ray structures of metal-free, dicobalt and dimanganese forms of soluble methane monooxygenase hydroxylase from *Methylococcus capsulatus* (Bath). *Biochemistry* 43:16263–76

24. Sazinsky MH, Lippard SJ. 2005. Product bound structures of the soluble methane monooxygenase hydroxylase from *Methylococcus capsulatus* (Bath): protein motion in the α-subunit. *J. Am. Chem. Soc.* 127:5814–25
25. Stenkamp RE. 1994. Dioxygen and hemerythrin. *Chem. Rev.* 94:715–26
26. Jasniewski AJ, Que L Jr. 2018. Dioxygen activation by nonheme diiron enzymes: diverse dioxygen adducts, high-valent intermediates, and related model complexes. *Chem. Rev.* 118:2554–92
27. Fox BG, Surerus KK, Münck E, Lipscomb JD. 1988. Evidence for a μ-oxo-bridged binuclear iron cluster in the hydroxylase component of methane monooxygenase: Mössbauer and EPR studies. *J. Biol. Chem.* 263:10553–56
28. Colby J, Dalton H. 1978. Resolution of the methane monooxygenase of *Methylococcus capsulatus* (Bath) into three components. *Biochem. J.* 171:461–68
29. Lund J, Woodland MP, Dalton H. 1985. Electron transfer reactions in the soluble methane monooxygenase of *Methylococcus capsulatus* (Bath). *Eur. J. Biochem.* 147:297–305
30. Fox BG, Liu Y, Dege JE, Lipscomb JD. 1991. Complex formation between the protein components of methane monooxygenase from *Methylosinus trichosporium* OB3b: identification of sites of component interaction. *J. Biol. Chem.* 266:540–50
31. Liu Y, Nesheim JC, Paulsen KE, Stankovich MT, Lipscomb JD. 1997. Roles of the methane monooxygenase reductase component in the regulation of catalysis. *Biochemistry* 36:5223–33
32. Kopp DA, Berg EA, Costello CE, Lippard SJ. 2003. Structural features of covalently cross-linked hydroxylase and reductase proteins of soluble methane monooxygenase as revealed by mass spectrometric analysis. *J. Biol. Chem.* 278:20939–45
33. Green J, Dalton H. 1985. Protein B of soluble methane monooxygenase from *Methylococcus capsulatus* (Bath): a novel regulatory protein of enzyme activity. *J. Biol. Chem.* 260:15795–801
34. Froland WA, Andersson KK, Lee S-K, Liu Y, Lipscomb JD. 1992. Methane monooxygenase component B and reductase alter the regioselectivity of the hydroxylase component-catalyzed reactions: a novel role for protein-protein interactions in an oxygenase mechanism. *J. Biol. Chem.* 267:17588–97
35. MacArthur R, Sazinsky MH, Kuehne H, Whittington DA, Lippard SJ, Brudvig GW. 2002. Component B binding to the soluble methane monooxygenase hydroxylase by saturation-recovery EPR spectroscopy of spin-labeled MMOB. *J. Am. Chem. Soc.* 124:13392–93
36. Lee SJ, McCormick MS, Lippard SJ, Cho U-S. 2013. Control of substrate access to the active site in methane monooxygenase. *Nature* 494:380–84
37. Sazinsky MH, Dunten PW, McCormick MS, DiDonato A, Lippard SJ. 2006. X-ray structure of a hydroxylase-regulatory protein complex from a hydrocarbon-oxidizing multicomponent monooxygenase, *Pseudomonas* sp. OX1 phenol hydroxylase. *Biochemistry* 45:15392–404
38. McCormick MS, Sazinsky MH, Condon KL, Lippard SJ. 2006. X-ray crystal structures of manganese(II)-reconstituted and native toluene/*o*-xylene monooxygenase hydroxylase reveal rotamer shifts in conserved residues and an enhanced view of the protein interior. *J. Am. Chem. Soc.* 128:15108–10
39. Bailey LJ, McCoy JG, Phillips GN Jr., Fox BG. 2008. Structural consequences of effector protein complex formation in a diiron hydroxylase. *PNAS* 105:19194–98
40. Liang AD, Wrobel AT, Lippard SJ. 2014. A flexible glutamine regulates the catalytic activity of toluene *o*-xylene monooxygenase. *Biochemistry* 53:3585–92
41. Sazinsky MH, Lippard SJ. 2015. Methane monooxygenase: functionalizing methane at iron and copper. *Met. Ions Life Sci.* 15:205–56
42. Lee SK, Nesheim JC, Lipscomb JD. 1993. Transient intermediates of the methane monooxygenase catalytic cycle. *J. Biol. Chem.* 268:21569–77
43. Liu Y, Nesheim JC, Lee S-K, Lipscomb JD. 1995. Gating effects of component B on oxygen activation by the methane monooxygenase hydroxylase component. *J. Biol. Chem.* 270:24662–65
44. Wang W, Lippard SJ. 2014. Diiron oxidation state control of substrate access to the active site of soluble methane monooxygenase mediated by the regulatory component. *J. Am. Chem. Soc.* 136:2244–47
45. Wallar BJ, Lipscomb JD. 2001. Methane monooxygenase component B mutants alter the kinetics of steps throughout the catalytic cycle. *Biochemistry* 40:2220–33

46. Zhang J, Lipscomb JD. 2006. Role of the C-terminal region of the B component of *Methylosinus trichosporium* OB3b methane monooxygenase in the regulation of oxygen activation. *Biochemistry* 45:1459–69
47. Liu KE, Valentine AM, Wang DL, Huynh BH, Edmondson DE, et al. 1995. Kinetic and spectroscopic characterization of intermediates and component interactions in reactions of methane monooxygenase from *Methylococcus capsulatus* (Bath). *J. Am. Chem. Soc.* 117:10174–85
48. Lee SK, Lipscomb JD. 1999. Oxygen activation catalyzed by methane monooxygenase hydroxylase component: proton delivery during the O–O bond cleavage steps. *Biochemistry* 38:4423–32
49. Brazeau BJ, Lipscomb JD. 2000. Kinetics and activation thermodynamics of methane monooxygenase compound Q formation and reaction with substrates. *Biochemistry* 39:13503–15
50. Tinberg CE, Lippard SJ. 2009. Revisiting the mechanism of dioxygen activation in soluble methane monooxygenase from *M. capsulatus* (Bath): evidence for a multi-step, proton-dependent reaction pathway. *Biochemistry* 48:12145–58
51. Banerjee R, Meier KK, Münck E, Lipscomb JD. 2013. Intermediate P* from soluble methane monooxygenase contains a diferrous cluster. *Biochemistry* 52:4331–42
52. Hendrich MP, Münck E, Fox BG, Lipscomb JD. 1990. Integer-spin EPR studies of the fully reduced methane monooxygenase hydroxylase component. *J. Am. Chem. Soc.* 112:5861–65
53. Priestley ND, Floss HG, Froland WA, Lipscomb JD, Williams PG, Morimoto H. 1992. Cryptic stereospecificity of methane monooxygenase. *J. Am. Chem. Soc.* 114:7561–62
54. Jin Y, Lipscomb JD. 2000. Mechanistic insights into C–H activation from radical clock chemistry: oxidation of substituted methylcyclopropanes catalyzed by soluble methane monooxygenase from *Methylosinus trichosporium* OB3b. *Biochim. Biophys. Acta* 1543:47–59
55. Brazeau BJ, Austin RN, Tarr C, Groves JT, Lipscomb JD. 2001. Intermediate Q from soluble methane monooxygenase hydroxylates the mechanistic substrate probe norcarane: evidence for a stepwise reaction. *J. Am. Chem. Soc.* 123:11831–37
56. Beauvais LG, Lippard SJ. 2005. Reactions of the peroxo intermediate of soluble methane monooxygenase hydroxylase with ethers. *J. Am. Chem. Soc.* 127:7370–78
57. Tinberg CE, Lippard SJ. 2010. Oxidation reactions performed by soluble methane monooxygenase hydroxylase intermediates H_{peroxo} and Q proceed by distinct mechanisms. *Biochemistry* 49:7902–12
58. Do LH, Hayashi T, Moenne-Loccoz P, Lippard SJ. 2010. Carboxylate as the protonation site in (peroxo)diiron(III) model complexes of soluble methane monooxygenase and related diiron proteins. *J. Am. Chem. Soc.* 132:1273–75
59. Banerjee R, Proshlyakov Y, Lipscomb JD, Proshlyakov DA. 2015. Structure of the key species in the enzymatic oxidation of methane to methanol. *Nature* 518:431–34
60. Lee SK, Fox BG, Froland WA, Lipscomb JD, Münck E. 1993. A transient intermediate of the methane monooxygenase catalytic cycle containing a $Fe^{IV}Fe^{IV}$ cluster. *J. Am. Chem. Soc.* 115:6450–51
61. Valentine AM, Tavares P, Pereira AS, Davydov R, Krebs C, et al. 1998. Generation of a mixed-valent Fe(III)Fe(IV) form of intermediate Q in the reaction cycle of soluble methane monooxygenase, an analog of intermediate X in ribonucleotide reductase R2 assembly. *J. Am. Chem. Soc.* 120:2190–91
62. Wilkinson EC, Dong YH, Zang Y, Fujii H, Fraczkiewicz R, et al. 1998. Raman signature of the Fe_2O_2 "diamond" core. *J. Am. Chem. Soc.* 120:955–62
63. Nesheim JC, Lipscomb JD. 1996. Large isotope effects in methane oxidation catalyzed by methane monooxygenase: evidence for C−H bond cleavage in a reaction cycle intermediate. *Biochemistry* 35:10240–47
64. Shu L, Nesheim JC, Kauffmann K, Münck E, Lipscomb JD, Que L Jr. 1997. An $Fe^{IV}{}_2O_2$ diamond core structure for the key intermediate Q of methane monooxygenase. *Science* 275:515–18
65. Rohde J-U, In J-H, Lim M-H, Brennessel WW, Bukowski MR, et al. 2003. Crystallographic and spectroscopic characterization of a nonheme Fe(IV) = O complex. *Science* 299:1037–39
66. Castillo RG, Banerjee R, Allpress CJ, Rohde GT, Bill E, et al. 2017. High-energy-resolution fluorescence-detected X-ray absorption of the Q intermediate of soluble methane monooxygenase. *J. Am. Chem. Soc.* 139:18024–33

67. Cutsail GE III, Banerjee R, Zhou A, Que L Jr., Lipscomb JD, DeBeer S. 2018. High-resolution extended X-ray absorption fine structure analysis provides evidence for a longer Fe···Fe distance in the Q intermediate of methane monooxygenase. *J. Am. Chem. Soc.* 140:16807–20
68. Xue G, De Hont R, Münck E, Que L Jr. 2010. Million-fold activation of the $[Fe_2(\mu\text{-}O)_2]$ diamond core for C–H bond cleavage. *Nat. Chem.* 2:400–5
69. Siegbahn PEM, Crabtree RH. 1997. Mechanism of C–H activation by diiron methane monooxygenases: quantum chemical studies. *J. Am. Chem. Soc.* 119:3103–13
70. Siegbahn PEM. 2001. O—O bond cleavage and alkane hydroxylation in methane monooxygenase. *J. Biol. Inorg. Chem.* 6:27–45
71. Mai BK, Kim Y. 2013. Theoretical studies for large tunneling and the hydrogen-transfer mechanism in the C–H activation of CH_3CN by the di(μ-oxo)diiron(IV) complex: a model for intermediate Q in soluble methane monooxygenase. *Chem. Eur. J.* 19:3568–72
72. Basch H, Musaev DG, Mogi K, Morokima K. 2001. Theoretical studies on the mechanism of the methane → methanol conversion reaction catalyzed by methane monooxygenase (MMO): the O-side versus N-side mechanisms. *J. Phys. Chem. A* 105:3615–22
73. Gherman BF, Dunietz BD, Whittington DA, Lippard SJ, Friesner RA. 2001. Activation of the C–H bond of methane by intermediate Q of methane monooxygenase: a theoretical study. *J. Am. Chem. Soc.* 123:3836–37
74. Musaev DG, Basch H, Morokuma K. 2002. Theoretical study of the mechanism of alkane hydroxylation and ethylene epoxidation reactions catalyzed by diiron bis-oxo complexes: the effect of substrate molecules. *J. Am. Chem. Soc.* 124:4135–48
75. Yoshizawa K. 2000. Two-step concerted mechanism for methane hydroxylation on the diiron active site of soluble methane monooxygenase. *J. Inorg. Biochem.* 78:23–34
76. Yoshizawa K. 2006. Nonradical mechanism for methane hydroxylation by iron-oxo complexes. *Acc. Chem. Res.* 39:375–82
77. Newcomb M, Le Tadic-Biadatti M-H, Chestney DL, Roberts ES, Hollenberg PF. 1995. A nonsynchronous concerted mechanism for cytochrome P-450 catalyzed hydroxylation. *J. Am. Chem. Soc.* 117:12085–91
78. Shestakov AF, Shilov AE. 1996. Five-coordinate carbon hydroxylation mechanism. *J. Mol. Catal. A* 105:1–7
79. Gherman BF, Lippard SJ, Friesner RA. 2005. Substrate hydroxylation in methane monooxygenase: quantitative modeling via mixed quantum mechanics/molecular mechanics techniques. *J. Am. Chem. Soc.* 127:1025–37
80. Fox BG, Borneman JG, Wackett LP, Lipscomb JD. 1990. Haloalkene oxidation by the soluble methane monooxygenase from *Methylosinus trichosporium* OB3b: mechanistic and environmental implications. *Biochemistry* 29:6419–27
81. Groves JT. 1985. Key elements of the chemistry of cytochrome P-450. The oxygen rebound mechanism. *J. Chem. Educ.* 62:928–31
82. Groves JT. 2006. High-valent iron in chemical and biological oxidations. *J. Inorg. Biochem.* 100:434–47
83. Valentine AM, Wilkinson B, Liu KE, Komarpanicucci S, Priestley ND, et al. 1997. Tritiated chiral alkanes as substrates for soluble methane monooxygenase from *Methylococcus capsulatus* (Bath): probes for the mechanism of hydroxylation. *J. Am. Chem. Soc.* 119:1818–27
84. Baik M-H, Gherman BF, Friesner RA, Lippard SJ. 2002. Hydroxylation of methane by non-heme diiron enzymes: molecular orbital analysis of C–H bond activation by reactive intermediate Q. *J. Am. Chem. Soc.* 124:14608–15
85. Guallar V, Gherman BF, Miller WH, Lippard SJ, Friesner RA. 2002. Dynamics of alkane hydroxylation at the non-heme diiron center in methane monooxygenase. *J. Am. Chem. Soc.* 124:3377–84
86. Choi S-Y, Eaton PE, Kopp DA, Lippard SJ, Newcomb M, Shen R. 1999. Cationic species can be produced in soluble methane monooxygenase-catalyzed hydroxylation reactions; radical intermediates are not formed. *J. Am. Chem. Soc.* 121:12198–99
87. Jin Y, Lipscomb JD. 1999. Probing the mechanism of C–H activation: oxidation of methylcubane by soluble methane monooxygenase from *Methylosinus trichosporium* OB3b. *Biochemistry* 38:6178–86

88. Valentine AM, LeTadic-Biadatti M-H, Toy PH, Newcomb M, Lippard SJ. 1999. Oxidation of ultrafast radical clock substrate probes by the soluble methane monooxygenase from *Methylococcus capsulatus* (Bath). *J. Biol. Chem.* 274:10771–76
89. Valentine AM, Stahl SS, Lippard SJ. 1999. Mechanistic studies of the reaction of reduced methane monooxygenase hydroxylase with dioxygen and substrates. *J. Am. Chem. Soc.* 121:3876–87
90. Brazeau BJ, Wallar BJ, Lipscomb JD. 2001. Unmasking of deuterium kinetic isotope effects on the methane monooxygenase compound Q reaction by site-directed mutagenesis of component B. *J. Am. Chem. Soc.* 123:10421–22
91. Klinman JP. 2006. The role of tunneling in enzyme catalysis of C–H activation. *Biochim. Biophys. Acta Bioenerg.* 1757:981–87
92. Zheng H, Lipscomb JD. 2006. Regulation of methane monooxygenase catalysis based on size exclusion and quantum tunneling. *Biochemistry* 45:1685–92
93. Carr CAM, Klinman JP. 2014. Hydrogen tunneling in a prokaryotic lipoxygenase. *Biochemistry* 53:2212–14
94. Siebrand W, Smedarchina Z. 2006. Mechanism of CH-bond cleavage catalyzed by enzymes. In *Isotope Effects in Chemistry and Biology*, ed. A Kohen, H-H Limbach, pp. 725–41. Boca Raton, FL: Taylor & Francis
95. Arciero DM, Lipscomb JD. 1986. Binding of ^{17}O-labeled substrate and inhibitors to protocatechuate 4,5-dioxygenase-nitrosyl complex: evidence for direct substrate binding to the active site Fe^{2+} of extradiol dioxygenases. *J. Biol. Chem.* 261:2170–78
96. Wolfe MD, Parales JV, Gibson DT, Lipscomb JD. 2001. Single turnover chemistry and regulation of O_2 activation by the oxygenase component of naphthalene 1,2-dioxygenase. *J. Biol. Chem.* 276:1945–53
97. Lipscomb JD, Sligar SG, Namtvedt MJ, Gunsalus IC. 1976. Autooxidation and hydroxylation reactions of oxygenated cytochrome $P450_{cam}$. *J. Biol. Chem.* 251:1116–24
98. Poulos TL. 2014. Heme enzyme structure and function. *Chem. Rev.* 114:3919–62
99. Pau MYM, Lipscomb JD, Solomon EI. 2007. Substrate activation for O_2 reactions by oxidized metal centers in biology. *PNAS* 104:18355–62
100. Rivard BS, Rogers MS, Marell DJ, Neibergall MB, Chakrabarty S, et al. 2015. Rate-determining attack on substrate precedes Rieske cluster oxidation during cis-dihydroxylation by benzoate dioxygenase. *Biochemistry* 54:4652–64
101. Komor AJ, Rivard BS, Fan R, Guo Y, Que L Jr., Lipscomb JD. 2017. CmlI *N*-oxygenase catalyzes the final three steps in chloramphenicol biosynthesis without dissociation of intermediates. *Biochemistry* 56:4940–50
102. Sutherlin KD, Rivard BS, Bottger LH, Liu LV, Rogers MS, et al. 2018. NRVS studies of the peroxide shunt intermediate in a Rieske dioxygenase and its relation to the native Fe(II) O_2 reaction. *J. Am. Chem. Soc.* 140:5544–59
103. Mitić N, Schwartz JK, Brazeau BJ, Lipscomb JD, Solomon EI. 2008. CD and MCD studies of the effects of component B variant binding on the biferrous active site of methane monooxygenase. *Biochemistry* 47:8386–97
104. Rinaldo D, Philipp DM, Lippard SJ, Friesner RA. 2007. Intermediates in dioxygen activation by methane monooxygenase: a QM/MM study. *J. Am. Chem. Soc.* 129:3135–47
105. Brazeau BJ, Wallar BJ, Lipscomb JD. 2003. Effector proteins from $P450_{cam}$ and methane monooxygenase: lessons in tuning nature's powerful reagents. *Biochem. Biophys. Res. Commun.* 312:143–48
106. Zhang J, Wallar BJ, Popescu CV, Renner DB, Thomas DD, Lipscomb JD. 2006. Methane monooxygenase hydroxylase and B component interactions. *Biochemistry* 45:2913–26
107. Brazeau BJ, Lipscomb JD. 2003. Key amino acid residues in the regulation of soluble methane monooxygenase catalysis by component B. *Biochemistry* 42:5618–31
108. Wang W, Liang AD, Lippard SJ. 2015. Coupling oxygen consumption with hydrocarbon oxidation in bacterial multicomponent monooxygenases. *Acc. Chem. Res.* 48:2632–39
109. Song WJ, Gucinski G, Sazinsky MH, Lippard SJ. 2011. Tracking a defined route for O_2 migration in a dioxygen-activating diiron enzyme. *PNAS* 108:14795–800

110. Smith TJ, Slade SE, Burton NP, Murrell JC, Dalton H. 2002. Improved system for protein engineering of the hydroxylase component of soluble methane monooxygenase. *Appl. Environ. Microbiol.* 68:5265–73
111. Puri AW, Owen S, Chu F, Chavkin T, Beck DAC, et al. 2015. Genetic tools for the industrially promising methanotroph *Methylomicrobium buryatense*. *Appl. Environ. Microbiol.* 81:1775–81
112. Yan X, Chu F, Puri AW, Fu Y, Lidstrom ME. 2016. Electroporation-based genetic manipulation in type I methanotrophs. *Appl. Environ. Microbiol.* 82:2062–69
113. Nagel ZD, Klinman JP. 2006. Tunneling and dynamics in enzymatic hydride transfer. *Chem. Rev.* 106:3095–118
114. Brandstetter H, Whittington DA, Lippard SJ, Frederick CA. 1999. Mutational and structural analyses of the regulatory protein B of soluble methane monooxygenase from *Methylococcus capsulatus* (Bath). *Chem. Biol.* 6:441–49
115. Gassner GT, Lippard SJ. 1999. Component interactions in the soluble methane monooxygenase system from *Methylococcus capsulatus* (Bath). *Biochemistry* 38:12768–85
116. Wang W, Iacob RE, Luoh RP, Engen JR, Lippard SJ. 2014. Electron transfer control in soluble methane monooxygenase. *J. Am. Chem. Soc.* 136:9754–62
117. Paulsen KE, Liu Y, Fox BG, Lipscomb JD, Münck E, Stankovich MT. 1994. Oxidation-reduction potentials of the methane monooxygenase hydroxylase component from *Methylosinus trichosporium* OB3b. *Biochemistry* 33:713–22
118. Liu KE, Lippard SJ. 1991. Redox properties of the hydroxylase component of methane monooxygenase from *Methylococcus capsulatus* (Bath): effects of protein B, reductase, and substrate. *J. Biol. Chem.* 266:12836–39. Erratum. 1991. *J. Biol. Chem.* 266:24859
119. Blazyk JL, Gassner GT, Lippard SJ. 2005. Intermolecular electron-transfer reactions in soluble methane monooxygenase: a role for hysteresis in protein function. *J. Am. Chem. Soc.* 127:17364–76
120. Friedle S, Reisner E, Lippard SJ. 2010. Current challenges of modeling diiron enzyme active sites for dioxygen activation by biomimetic synthetic complexes. *Chem. Soc. Rev.* 39:2768–79
121. Karlin KD, Lippard SJ, Valentine JS, Burrows CJ. 2015. Solving 21st century problems in biological inorganic chemistry using synthetic models. *Acc. Chem. Res.* 48:2659–60